Seatific

Research Article

Numerical investigation of the resistance and static drift condition of the autosub submarine

Sare Nur ÇIPLAKKAYA⬤**, Yasemin ARIKAN ÖZDEN***⬤

Department of Naval Architecture and Marine Engineering, Faculty of Naval Architecture and Maritime, Yildiz Technical University, Istanbul, Türkiye

ABSTRACT

This study involves the force and moment calculations using the scaled and full-scale geometries of the Autosub submarine. The scale factor of the submarine is used as 1.346 according to the model size used in the experiments. Computational fluid dynamics calculations have been performed using RANS equations and the k-ω turbulence model. The resistance analyses have been conducted for speeds ranging from 0 to 2 m/s. Static drift analyses have been conducted between the range of 0º to 10º degrees drift angles at 2 degrees intervals. A mesh independence study has been carried out to determine the adequate mesh density. The mesh structure has been determined in the analyses for 6 degrees of drift angle and this mesh structure is used for other drift angles, and the results have been compared with experimental results from the open literature. Full-scale resistance analyses have been conducted, and the calculated resistance forces have been compared with the experimental and empirical data. The force and moment values obtained from static drift and resistance analyses are found to be consistent with experimental results presented in the literature.

Cite this article as: Çıplakkaya SN, Arıkan Özden Y. Numerical investigation of the resistance and static drift condition of the autosub submarine. Seatific 2023;3:2:71–84.

1. INTRODUCTION

One of the factors that determine the design of submarines is their maneuvering performance. During the process of determining maneuvering performance, it is crucial to calculate the maneuvering coefficients that represent the hydrodynamic effects. Obtaining the hydrodynamic coefficients which are part of the equations of motion is one of the most important parts for the maneuvering calculations (Cardenas et al., 2019). Computational fluid dynamics, empirical, and experimental methods are used

to obtain the hydrodynamic characteristics of submarines. Hydrodynamic coefficients are usually obtained through experimental or numerical simulations. Experiments enable the direct determination of coefficients by making measurements, but due to the high cost and difficulty of experiments, numerical simulations are becoming increasingly popular. There are three main conditions at submarine's motion; acceleration, cruise and rotating at constant angular velocity. These three conditions should be investigated in order to obtain the maneuvering characteristics. The hydrodynamic forces due to acceleration effects

*Corresponding author.
*E-mail address: yarikan@yildiz.edu.tr

are calculated through planar motion mechanism (PMM) experiments. The hydrodynamic forces and moments which occur at cruise are determined by towing tank tests while the angular velocity effects are carried out by rotating arm experiments (Efremov et al., 2019). Ship model testing experiments have different methods of calculating the hydrodynamic coefficients. For each method, the calculation methods differ. PMM is a hydrodynamic test system which allows to impose static drift and dynamic oscillating motions to a surface ship or submarine model. On the other hand, the rotating arm test, which is a different test setup, is used to obtain coefficients while the model is rotating with a constant angular velocity. To measure straight motion values such as longitudinal and lateral forces, the towing tank test are conducted. Thus, coefficients for drag, pitch or yaw angle are measured. Since in towing tank tests linear movements are obtained, measurements related to angular velocity cannot be obtained. This is what separates PMM test from the rotating arm test. The use of these test setups have a very important place in obtaining the hydrodynamic coefficients needed while designing a submarine (Saeidinezhad et al., 2015).

In this study, the Autosub underwater vehicle (AUV) is used which is a submarine developed by the British National Oceanography Centre. This submarine is commonly used by oceanographers for scientific research. The Autosub submarine is capable of staying underwater for extended periods of time and measures the physical, chemical, and biological properties of the underwater environment through various sensors. It is used for a variety of missions, such as exploring various geological features like underwater volcanoes, mountains, and canyons by measuring factors such as ocean temperature, salinity, and water quality. Additionally, it is used to examine and monitor underwater biological life. Furthermore, it is also used to investigate human-induced pollution and natural disasters, such as studying the effects of oil spills or tsunamis. Due to its ability to stay underwater for extended periods of time, the Autosub submarine has become an important tool in ocean sciences and has been used in numerous studies in this field.

The Autosub submarine is also a good validation tool used for submarine maneuvering studies since there are comprehensive model test results shared in the open literature. Model tests for the Autosub submarine have been performed on a model scaled by the scaling factor of 1.346 by Kimber & Marshfield (1993) at the HASLAR facility (270 m × 12.2 m × 5.5 m deep). Further tests were performed by Fallows (2004) on a 2.5 m scale model of the Autosub submarine at the Solent University Towing Tank (60 m × 3.7 m × 1.8 m deep). Experimental results in the open literature for the Autosub submarine are presented for submarines of different scale. Resistance results are presented for the full scale submarine while the PMM and rotating arm results are presented in non-dimensional form by the use of the

scaled submarine model. The cruise speed of the Autosub is 2 m/s at full-scale. Kimber & Marshfield (1993) used in the scaled model a velocity magnitude of 2.69 m/s to obtain the same turbulence specification. Static drift tests are conducted at ±0 degree to ±10 degrees with an increment of 2 degrees (Kimber & Marshfield, 1993). Fallows (2004) in his PhD thesis shares a description of the experiments conducted in Southampton Institute Towing Tank. The full scale sea trials have been described in his study and experimental results have been shared (Fallows, 2004).

Pioneering studies for experimental studies concerning UWV's date back to the DARPA Suboff project where comprehensive model experiments are conducted. The DARPA Suboff Submarine is designed and recommended as a benchmark submarine model by Groves et al. (1989). The stability and control characteristics of the DARPA Suboff submarine model have been presented by Roddy (1990). There is a very large literature concerning the experimental and numerical investigation for the resistance prediction of underwater vehicles. Studies where the resistance of the generic forms like DARPA Suboff, BB2 Joubert, C-Scout are obtained experimentally (Crook, 1990; Roddy, 1990; Liu & Huang ,1998; Carrica et al., 2016; Thomas et al., 2003; Thomas et al., 2003; Mackay, M., 1988) and numerically (Bull, 1996; Anckermann, 2008; Fell, 2009; McDonald & Whitfield, 1996; Alin et al., 2010; Chase & Carrica, 2013; Carrica et al., 2019) can be mentioned as pioneering studies.

The estimation of the maneuvering characteristics of an underwater vehicle is a challenging problem with various methods developed to solve this problem (Kırıkbaş et al., 2021a, 2021b). Literature concerning the numerical determination of the hydrodynamic derivatives for maneuvering models date back to Davidson &Ship (Davidson & Schiff, 1946). After Abkowitz (1964) who extended higher order terms for surface ships, Gertler& Hagen (1967) introduced the first model for submerged body. With the increase of computational power, computational fluid dynamics calculations have spread. Toxopeus & Vaz (2009) have carried out a study where the DARPA Suboff submarine model is used to investigate numerically the flow at different drift angles around the bare hull configuration. They used their own computational fluid dynamics code by implementing different turbulence models and conducted a verification and validation study (Toxopeus & Vaz, 2009). In another study Vaz et al. (2010) calculated the maneuvering forces and moments of the DARPA SUBOFF AFF-1 and AFF-8 configurations for 0° and 18° drift angles by using two viscous-flow solvers. The influence of different turbulence models namely, RANS (Reynolds-Averaged-Navier-Stokes) and DDES (Delayed-Detached-Eddy-Simulation) methods on the calculation of forces and moments were investigated (Vaz et al., 2010). Other studies where the static drift characteristics of the DARPA Suboff Submarine are investigated are Duman et al. (2018) where the static drift simulations of DARPA Suboff bare hull form have been carried out to

calculate the hydrodynamic forces and moment acting on the hull in the horizontal plane (Duman et al., 2021). Atik (2021) who investigated the suitable solution mesh and turbulence model for the DARPA SUBOFF submarine AFF-1 hull form by performing static drift test simulations (Atik, 2021). Kahramanoglu (2023) who has examined the scale effects on the horizontal maneuvering derivatives for three different scales for the fully appended DARPA Suboff submarine (Kahramanoglu, 2023).

Maneuvering studies on the Autosub submarine using computational fluid dynamics calculations are as follows. By providing a comprehensive understanding of complex systems, Fallows (2004) outlined an approach to enhance the performance of UWV systems that are already in use. He used Taguchi experimental methods and made complementary sets of measurements in the laboratory on the full scale Autosub submarine. His study presented a method for developing a propulsion system for an AUV, such as the Autosub submarine. He presented about the generic attributes of these systems and their requirements.

Wu et al. in their study aimed to reduce the total resistance of the Autosub submarine. For this purpose, simulations of microbubbles were carried out. When the bubbles passed close to the hull of the submarine, it caused a decrease in the density of the fluid and turbulence viscosity. It has been shown that a 50% improvement in the total resistance was achieved in submarines (Wu et al., 2006).

In the study of Philips et al., the focus has been on evaluating the hull resistance of three different Autosub submarines, each designed with distinct shapes and sizes. The objective was to calculate the resistance experienced by these vehicles during their underwater missions. By utilizing CFD, the researchers were able to simulate the fluid flow around the Autosub submarine bodies and to accurately calculate the resistance values. The calculated resistance values were then compared with available experimental data obtained from physical tests and measurements. The results showed a favorable level of agreement between the calculated and experimental resistance values, indicating the reliability and accuracy of the CFD method (Phillips et al., 2007).

Using steady-state computational fluid dynamics (CFD), Phillips et al. effectively replicated experiments which are known as rotating arm test and towing tank test to obtain steady-state hydrodynamic derivatives for a torpedo-style Autosub underwater vehicle (AUV). The predictions demonstrated excellent agreement in estimating sway forces, although there was a slight overestimation in induced drag and yaw moments. In addition, numerical methods accurately obtained the dynamic stability limits of the submarine, in close agreement with the experimental measurements (Phillips et al., 2010).

In another study Phillips et al. calculated the resistance and hydrodynamic coefficients of the Autosub model, the CFD method used for steady-state conditions was used to successfully reproduce horizontal towing tank and rotating arm experiments for a torpedo-style Autosub, and steady-state hydrodynamic derivatives were derived. While there was a very good match for the prediction of the sideways force, the induced resistance and yaw moment were found to be slightly higher than obtained. (Phillips et al., 2011). In the study of Joung et al. an Autosub concept design model was created and subjected to analysis using a commercial CFD program to evaluate its resistance characteristics. The CFD analysis provided measurements of pressure and velocity distribution around the submarine, as well as resistance measurements. Additionally, the analyses were expanded to investigate the effects of adjusting the sail and communication transducer positions, as well as the angle of attack of the propulsion nozzle, in order to optimize the Autosub's design and minimize the resistance. The CFD results were validated by comparing the results with the ITTC 1957 correlation line. The study demonstrated that CFD can effectively estimate the total resistance of complex-shaped submarines. To expedite convergence, an automated mesh generation technique incorporating boundary layer inclusion was employed. Significant reductions in convergence time were achieved by examining object function and changing time of per iteration. It has been shown by sensitivity analysis that the angle of attack of the nozzle has a significant effect on the resistance value (Joung et al., 2012).

Aslan in his master thesis investigated the hydrodynamic coefficients of the DARPA Suboff and the Autosub submarine by means of static drift and rotating arm calculations. CFD calculations were performed and a good agreement between numerical and experimental results was achieved (Aslan, 2013). Can in his master thesis calculated the static drag coefficients of the DARPA Suboff submarine and the Autosub underwater vehicle. In this research, the computational fluid dynamics (CFD) method was employed, and data regarding the static drift and rotating arm calculations were made. Steady and unsteady rotating arm calculations were performed. The obtained hydrodynamic coefficients values were compared with the results of the experiments presented in the open literature, and the maximum error rate was presented as 10% (Can, 2014).

In this study the Autosub 3 geometry is used. The full-scale submarine has a length of 7 meter, a diameter of 0.9 meter and a speed range of 1 to 2 m/s. The aim of this study is to investigate the resistance and the static drift conditions of the Autosub submarine through CFD analysis. The yaw moments, sway forces and surge forces are investigated. Static drift conditions for different angles of attack are calculated for the scaled and resistance for different forward speed are obtained for the full-scale model of the Autosub. A mesh independency and a validation study has been done to determine an adequate mesh structure.

This study has been done with the use of the computational fluid dynamics software Simcenter STAR-CCM+ which is a commercial software based on finite volume method to

calculate the transport of physical quantities on a discretized mesh. For modelling the fluid flow the Navier–Stokes equations are solved in each of the cells. The steady hydrodynamic analyses have been done at different drift angles by using the software. A mesh independency study has been done to determine the mesh structure that will be used in the analyses with 0,2,4,6,8 and 10 degrees of static drift angle. The case for 6 degrees drift angle has been selected for the mesh independency study. Five different mesh structure has been generated with different mesh element sizes. The result of these five analyses has been compared with the experimental results given in Phillips et al. (2007). As a result of this mesh independence study the mesh size that gives the results compatible with the experimental results has been selected. This selected mesh structure has been used while computing the other analyses.

2.METHODOLOGY

2.1. Coordinate System
In axes known as body-fixed, the origin is positioned to be at the center of gravity of the submarine. The X-axis shows the nose of the submarine. The y-axis is drawn towards the starboard side, while the z-axis is towards the downside of the submarine. The body-fixed axes are used as above and the space-fixed axes are presented in Figure 1 (Zhao et al., 2022).

2.2. Motion Parameters
The primary motion parameters of a submarine consist of the linear velocity U and the angular velocity Ω while investigating in a coordinate system which is body-fixed. The velocity components of the submarine are lettered as linear velocity and angular velocity, respectively, as u and p in the x-axis, v and q in the y-axis, and w and r in the z-axis, as seen in Figure 1. These velocity magnitudes are the components of the linear U velocity and the angular ω velocity of the submarine. It can be calculated with the help of the submarine speed and the angles of the submarine (Zhao et al., 2022).
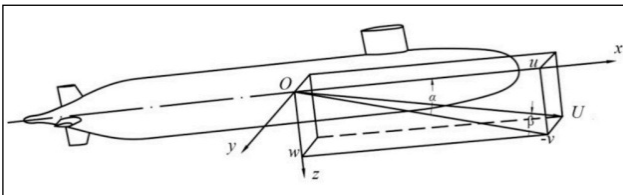

Figure 1. The coordinate systems (Zhao et al., 2022).

Equation 1 shows how the transformation mentioned above is applied.

$$u = U cos\beta cos\alpha, v = -U sin\beta, w = U cos\beta sin\alpha \quad (1)$$

$$u' = \frac{u}{U} = cos\beta cos\alpha, v' = \frac{v}{U} = sin\beta, w' = \frac{w}{U} = cos\beta sin\alpha$$

Equation (2) displays the values of the three components of angular velocity (p, q, and r) when the sail is positioned horizontally on the bottom.

$$p = sin\Omega\alpha, q = -\Omega cos\alpha sin\psi, r = -\Omega cos\alpha cos\psi \quad (2)$$

$$p' = \frac{pL}{U}, q' = \frac{qL}{U} = sin\beta, r' = \frac{rL}{U}$$

Equation (3) provides the values of the three components of angular velocity (p, q, and r) when the sail is positioned vertically on the starboard side.

$$p = -\Omega sin\beta, q = \Omega cos\beta cos\psi, r = -\Omega cos\beta sin\psi \quad (3)$$

$$p' = \frac{pL}{U}, q' = \frac{qL}{U} = sin\beta, r' = \frac{rL}{U}$$

A submarine gets subjected to many different forces during operation. These forces are lift force, weight force, drag force, propeller thrust and inertia forces. Test rigs generally measure 6 force components. These forces are labeled as X, Y, Z forces and K, M, N moments on the x, y, z axes, respectively. As is known from fluid mechanics, one of the forces that produce hydrodynamic effects are viscous forces. The measurements in the tests made provide the hydrodynamic forces resulting from the viscous effects and thus the coefficients to be obtained. The movements of the submarine are shown in Figure 2 along with their names (Zhao et al., 2022).
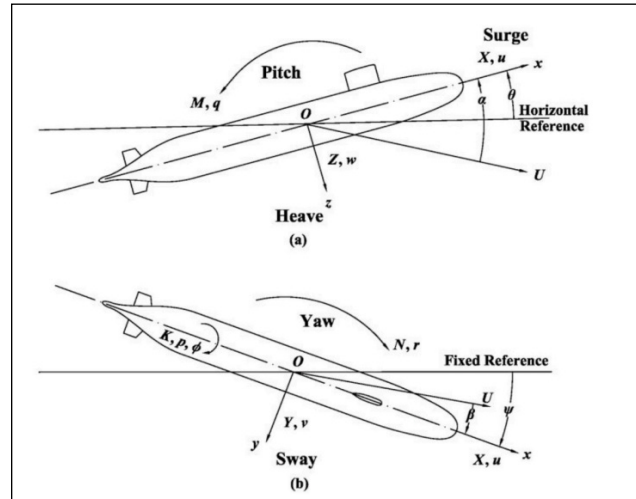

Figure 2. The motion of a submarine: (a) vertical plane; (b) horizontal plane (Zhao et al., 2022).

2.3. Maneuverability equations
Newton's second law can be used to derive equations of motion. The equations of motion with six degrees of freedom can be obtained as follows.

$$m[\dot{u} - vr + wq - x_G(q^2 + r^2) + y_G(pq - \dot{r}) + z_G(pr + \dot{q})] = F_x \quad (4)$$

$$m[\dot{v} - wp + ur - y_G(r^2 + p^2) + z_G(qr - \dot{p}) + x_G(qp + \dot{r})] = F_y \quad (5)$$

$$m[\dot{w} - uq + vp - z_G(p^2 + q^2) + x_G(rp - \dot{q}) + y_G(rp + \dot{p})] = F_z \quad (6)$$

$$I_x\dot{p} + (I_z - I_y)qr - I_{xz}(\dot{r} + pq) + I_{yz}(r^2 - q^2) + I_{xy}(pr - \dot{q}) + m[y_G(\dot{w} - uq + vp) - z_G(\dot{v} - wp + ur)] = M_x \quad (7)$$

$$I_y\dot{q} + (I_x - I_z)rp - I_{yx}(\dot{p} + qr) + I_{zx}(p^2 - r^2) + I_{yz}(qp - \dot{r}) + m[z_G(\dot{u} - vr + wq) - x_G(\dot{w} - uq + vp)] = M_y \quad (8)$$

$$I_z\dot{r} + (I_y - I_x)pq - I_{zy}(\dot{q} + rp) + I_{xy}(q^2 - p^2) + I_{zx}(rq - \dot{p}) + m[x_G(\dot{v} - wp + ur) - y_G(\dot{u} - vr + wq)] = M_z \quad (9)$$

The velocities that the submarine has during its operation are affected by the rotational velocities. These effects are expressed by the nonlinear parts of the equations. However, the assumption made in this study is that these effects are negligible. This means that the results do not take into account the resistance of cross-flows and unsteady viscous effects (Zhao et al., 2022). When the equations are arranged in line with this approach, the following equations are obtained.

Surge:

$$\frac{\rho}{2}l^4[X'_{qq}q^2 + X'_{rr}r^2 + X'_{rp}rp] + \frac{\rho}{2}l^3[X'_{\dot{u}}\dot{u} + X'_{vr}vr + X'_{wq}wq] + \frac{\rho}{2}l^2[X'_{uu}u^2 + X'_{vv}v^2 + X'_{ww}w^2] +$$
$$\frac{\rho}{2}l^2u^2[X'_{\delta e\delta e}\delta e^2 + X'_{\delta r\delta r}\delta r^2 + X'_{\delta a\delta a}\delta a^2] - (W - B)\sin\theta = X \quad (10)$$

Sway:

$$\frac{\rho}{2}l^4[Y'_{\dot{r}}\dot{r} + Y'_{\dot{p}}\dot{p} + Y'_{p|p|}p|p| + Y'_{pq}pq + Y'_{qr}qr] + \frac{\rho}{2}l^3[Y'_{\dot{v}}\dot{v} + Y'_{vq}vq + Y'_{wp}wp + Y'_{wr}wr] +$$
$$\frac{\rho}{2}l^3[Y'_{r}ur + Y'_{r|\delta r|}|r|\delta r + Y'_{v|r|}\frac{v}{|v|}(v^2 - w^2)^{\frac{1}{2}}|r|] + \frac{\rho}{2}l^2[Y'_{v}uv + Y'_{v|v|}v(v^2 - w^2)^{\frac{1}{2}}] +$$
$$\frac{\rho}{2}l^2[Y'_{vw}vw + Y'_{\delta r}u^2\delta r^2] + (W - B)\cos\theta\sin\phi = Y \quad (11)$$

Heave:

$$\frac{\rho}{2}l^4[Z'_{\dot{q}}\dot{q} + Z'_{pp}pp^2 + Z'_{rr}rr^2 + Z'_{rp}rp] + \frac{\rho}{2}l^3[Z'_{\dot{w}}\dot{w} + Z'_{vp}vp + Z'_{vr}vr] +$$
$$\frac{\rho}{2}l^3[Z'_{q}uq + Z'_{q|\delta e|}u|q|\delta e + Z'_{w|q|}\frac{w}{|w|}(v^2 + w^2)^{\frac{1}{2}}|q|] +$$
$$\frac{\rho}{2}l^2[Z'_{w}uw + Z'_{w|w|}w(v^2 + w^2)^{\frac{1}{2}} + \frac{\rho}{2}l^2[Z'_{|w|}u|w| + Z'_{ww}|w(v^2 + w^2)^{\frac{1}{2}}|] +$$
$$\frac{\rho}{2}l^2[Z'_{vv}v^2 + Z'_{\delta e}u^2\delta e + Z'_{\delta a}u^2\delta a] + (W - B)\cos\theta\cos\phi = Z \quad (12)$$

Roll:

$$\frac{\rho}{2}l^5[K'_{\dot{p}}\dot{p} + K'_{\dot{r}}\dot{r} + K'_{p|p|}p|p| + K'_{pq}pq + K'_{qr}qr] + \frac{\rho}{2}l^4[K'_{\dot{v}}\dot{v} + K'_{r}ur + K'_{p}up] +$$
$$\frac{\rho}{2}l^4[K'_{vq}vq + K'_{wp}wp + K'_{wr}wr] + \frac{\rho}{2}l^3[K'_{uv}uv + K'_{v|v|}v(v^2 + w^2)^{\frac{1}{2}}] +$$
$$\frac{\rho}{2}l^3[K'_{vw}vw + K'_{\delta r}u^2\delta r + K'_{\delta a}u^2\delta a] + (y_G W - y_B B)\cos\theta\sin\phi = K \quad (13)$$

Pitch:

$$\frac{\rho}{2}l^5[M'_{\dot{q}}\dot{q} + M'_{pp}pp^2 + M'_{rr}rr^2 + + M'_{rp}rp + M'_{q|q|}q|q|] + \frac{\rho}{2}l^4[M'_{\dot{w}}\dot{w} + M'_{vp}vp + M'_{vr}vr] +$$
$$\frac{\rho}{2}l^4[M'_{q}uq + M'_{q|\delta e|}u|q|\delta e + M'_{w|q|}\frac{w}{|w|}(v^2 + w^2)^{\frac{1}{2}}|q|] + \frac{\rho}{2}l^3[M'_{w}uw + M'_{w|w|}w(v^2 + w^2)^{\frac{1}{2}}] -$$
$$\frac{\rho}{2}l^3[M'_{|w|}u|w| + M'_{ww}|w(v^2 + w^2)^{\frac{1}{2}}|] + \frac{\rho}{2}l^3[M'_{vv}v^2 + M'_{\delta e}u^2\delta e + M'_{\delta a}u^2\delta a] -$$
$$(x_G W - x_B B)\cos\theta\cos\phi - (z_G W - z_B B)\sin\theta = M \quad (14)$$

Yaw:

$$\frac{\rho}{2}l^5[N'_{\dot{r}}\dot{r} + N'_{\dot{p}}\dot{p} + N'_{r|r|}r|r| + N'_{pq}pq + N'_{qr}qr] + \frac{\rho}{2}l^4[N'_{\dot{v}}\dot{v} + N'_{vq}vq + N'_{wp}wp + N'_{wr}wr] +$$
$$\frac{\rho}{2}l^4[N'_{r}ur + N'_{p}up + N'_{r|\delta r|}u|r|\delta r + N'_{v|r|}|(v^2 + w^2)^{\frac{1}{2}}|r|] + \frac{\rho}{2}l^3[N'_{v}uv + N'_{v|v|}|v(v^2 + w^2)^{\frac{1}{2}}|] +$$
$$\frac{\rho}{2}l^3[N'_{vw}vw + N'_{\delta r}u^2\delta r] + (x_G W - x_B B)\cos\theta\sin\phi - (y_G W - y_B B)\sin\theta = N \quad (15)$$

Sway force and yaw moment acting on a model can be measured by drift experiments which can be done with a submarine model. Gaining a yaw moment and sway velocity to the model creates a force and moment. The rate coefficients Y_v and N_v can be obtained with the help of the velocity versus force graphs obtained as a result of these tests repeated at different sway velocities.

2.4. The Reynolds-Averaged Navier-Stokes (RANS) Equations

ANSYS FLUENT is utilized to model the fluid dynamics surrounding Autosub, employing the incompressible and isothermal Reynolds Averaged Navier-Stokes (RANS) equations (17). This computational approach aimed to ascertain the Cartesian flow field (ui = u, v, w) and pressure (p) of the water surrounding the hull of an Autonomous Underwater Vehicle (AUV).

$$\frac{\partial U_i}{\partial x_i} = 0 \quad (16)$$

$$\frac{\partial U_i U_j}{\partial x_j} = -\frac{1}{\rho}\frac{\partial P}{\partial x_i} + \frac{\partial}{\partial x_j}\left\{v\left(\frac{\partial U_i}{\partial x_j} + \frac{\partial U_j}{\partial x_i}\right)\right\} - \frac{\partial \overline{u'_i u'_j}}{\partial x_j} + f_i \quad (17)$$

The k-ω model is one of the most preferred turbulence models. In this problem, the "k-ω SST" model was used. The k-ω SST model employs the vortex viscosity approach to model the boundary layer, ensuring a more accurate inclusion of shear forces in the equations. Atik (2021) in her study where she investigated the static drift performance of the DARPA Suboff submarine AFF-1 configuration, stated that all turbulence models gave close results at small angles, while after 8 degrees of drift angle the SST k-ω turbulence model gave the closest results.

2.5. Presentation of Forces and Moments

To convert the acquired forces and moments into non-dimensional values, the equations 18-19 as outlined in the SNAME (1950) proposal are used. The X, Y, and Z axis resistive forces are made non-dimensional by applying the following formula.

$$X', Y', Z' = \frac{X, Y, Z}{\frac{1}{2} \rho V_0^2 L_0^2} \tag{18}$$

K, M, N are the moments that occur around the X, Y, Z axis, respectively. To make non- dimensionalization of these moments, the following formula is used.

$$K', M', N' = \frac{K, M, N}{\frac{1}{2} \rho V_0^2 L_0^3} \tag{19}$$

3. GEOMETRY OF BODIES

The Autosub autonomous submarine model has evolved from the past to the present with the advancement of technology. The National Oceanography Centre (NOC) in Wormley initiated a program to develop scientific applications for autonomous underwater vehicles. The Autosub submarine vehicle, which has multiple geometries tailored to different purposes, was designed according to its usage. The Autosub submarine has an approximate length of 7 meters and a diameter of 0.9 meters. The Autosub submarine model to be used in this study has a scale factor of 1.346. The geometric characteristics of the Autosub submarine model are provided in Table 1 (Can, 2014). The image of the created Autosub model can be seen in Figure 3 and Figure 4.

Table 1. Geometric Properties of the Autosub Model (Can, 2014)

Description	Abbreviation	Value
Length overall	L_{OA}	5.2 m
Diameter	D	0.669 m
Nose Length	L_N	1.022 m
Nose shape		Elliptic
Body Length	L_B	2.020 m
Body Cross Section Area	S_B	0.352 m²
Aft Body Length	L_{AFT}	1.799 m
CG Distance from Nose	CG_N	2.310 m
Tail Span	B_t(Tip to Tip)	0.854 m
Tail Tip Chord Length	c	0.200 m
Sweep Angle (Leading Edge)	degrees	14.40°
Sweep Angle (Trailing Edge)	degrees	0°
Tail Airfoil		NACA0015

4. NUMERICAL CALCULATIONS

4.1 Mesh Independence Study

The aim of the mesh independence study is to create a mesh structure that would provide calculations with a reasonable level of error in terms of the conducted analyses and, at the same time, minimize the number of elements to reduce the computational cost. In line with this objective, a mesh independence study is carried out. Since experimental data for the Autosub submarine vehicle are available, the numerical results are validated with the experimental results.

4.1.1 Domain & Boundary Conditions

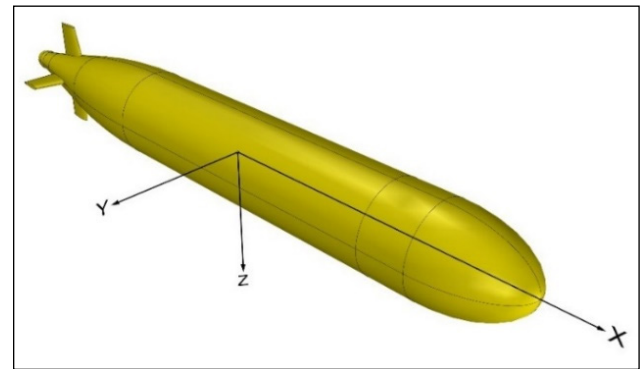The dimensions of the cylindrical geometry created for the domain are as shown in Figure 5. The domain is created

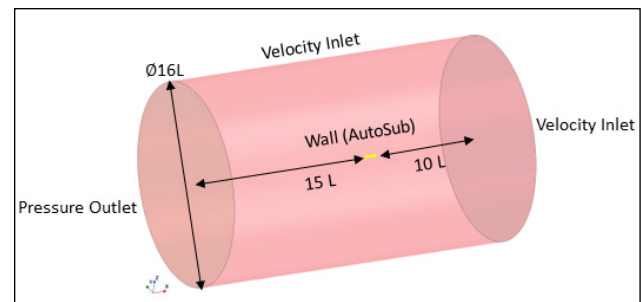**Figure 4.** Autosub Geometry Perspective View.

Figure 5. Boundary Conditions for the Static Drift Tests on Star CCM+

Figure 3. Autosub Geometry Top View and Back View.

with a size that is 10 times the length of the submarine at the front and 15 times at the back. In addition, the diameter of the cylinder is determined to be 16 times the length of the submarine. Velocity inlet is defined on the front surface and side surfaces of the cylindrical volume. On the back surface, a pressure outlet boundary condition is defined with a pressure value of 0 Pa. For each drift angle, a velocity vector is determined and assigned to the velocity inlet surfaces.

4.1.2 Physical Model

Steady-State RANS equations are used in all calculations. Viscous effects within the boundary layer are obtained using wall functions in the conducted analyses. In the analyses the k-ω SST turbulence model is used, the first layer thickness is created to satisfy the condition 30 < y⁺ < 300.

To obtain the desired wall distance y+ the Equation (20) is used to calculate the thickness of the first layer.

$$\Delta y = L\Delta y^+ \sqrt{80} R_n^{-13/14} \tag{20}$$

The calculation of the layer thickness is determined based on the Reynolds number, as given in Equation (21) (Phillips et al., 2007). A total number of 10 layers are created. The boundary layer for a blunt body can be estimated using the following equation:

$$\delta = 0.035 L R_n^{-1/7} \tag{21}$$

4.1.3. Mesh Structure

In this study, five different mesh densities with varying element counts are created. Figure 6 show the volume meshes of the Autosub submarine. The element size follows an increase ratio of $\sqrt{2}$, as recommended by the ITTC (International Towing Tank Conference) guidelines. (ITTC Resistance Committee, 2017).

It can be observed that the mesh is refined near the Autosub model. This refinement aims to better solve the flow region in close proximity to the model, ensuring more accurate analysis in that area.

4.1.4 Uncertainty Study

The method that known as (GCI) Grid Convergence Index has been used on verification of the grid structure. The uncertainty analysis has been conducted for the scenario with 6-degrees drift angle. The velocity vector is calculated
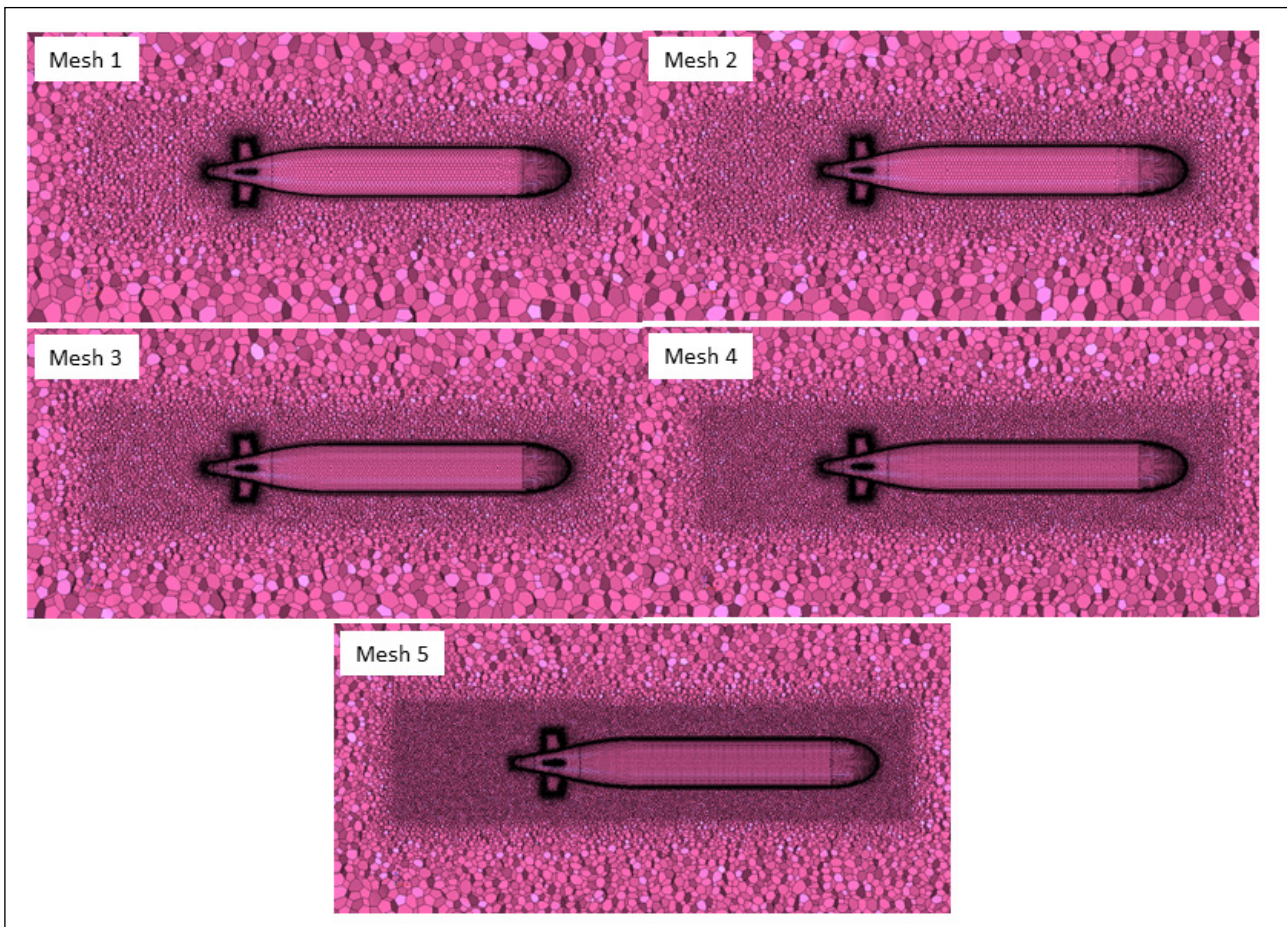

Figure 6. Mesh Structures.

Table 2. Static Drift Results for 6 degrees drift angle

6 Degrees Static Drift Results							
	Cell Number	Y	Y'	N	N'	Error (%) Y'	Error (%) N'
EXP	-	298,9826	0,003062	274,0047	0,000540	-	-
Mesh 1	794489	324,8269	0,003326	310,7741	0,000612	8,6440	13,4193
Mesh 2	1170857	319,5991	0,003273	308,1391	0,000607	6,8956	12,4576
Mesh 3	1841095	305,4607	0,003128	303,9573	0,000599	2,1667	10,9314
Mesh 4	2952064	301,7904	0,003090	302,1399	0,000595	0,9391	10,2682
Mesh 5	5639856	300,4577	0,003077	300,3557	0,000591	0,4934	9,6169

based on this angle. Table 2 presents the element count, results and deviations according to experimental results for different mesh densities. The analyses are conducted on a Windows operating system using a 4-core processor. The connection between the forces at 6 degrees of static drift and the mesh structure can be seen in Figure 7. Figure 8 shows the connection of the moments at 6 degrees of static drift with the mesh structure.

Roache (1994) presented the Grid Convergence Index (GCI) method in his study. While there are many different methods, this method focuses on mesh refinement, which is one of the important areas in CFD studies. This method, which is presented to reduce the complexity in grid refinement studies, has been used in many different studies and
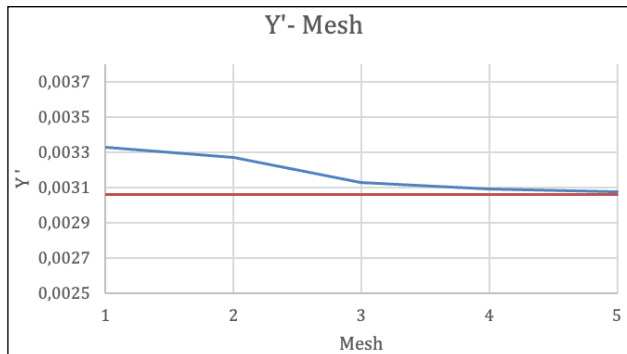
Figure 7. Sway Force Y' for drift angle 6 degrees.
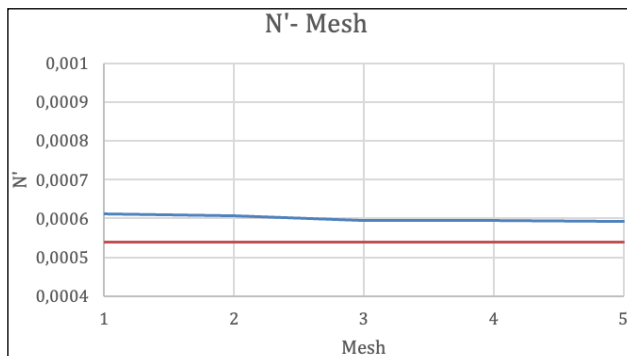
Figure 8. Yaw Moment N' for drift angle 6 degrees.

has been accepted by researchers. The mentioned method was edited by Celik et al. (2008) and presented again. In this study this edited method of GCI has been used as follows. Mesh size can be found by Equation (22).

$$h = \left[\frac{1}{N} \Sigma_{i=1}^{N} (\Delta V_i) \right]^{\frac{1}{3}} \tag{22}$$

N is the number of cells and V_i is the volume of i th cell.

Grid refinement factor can be found with Equation (23). h_1, h_2 and h_3 is calculated with the help of Equation (22) for fine, medium and coarse grids, respectively.

$$r_{21} = \frac{h_2}{h_1} \; ; \; r_{32} = \frac{h_3}{h_2} \tag{23}$$

After calculating the refinement factors between fine and medium; medium and coarse, we can calculate the apparent order which is p in Equation (24).

$$p = \frac{1}{ln \, ln \, (r_{21})} \left| ln \, ln \, \left| \frac{\varepsilon_{32}}{\varepsilon_{21}} \right| + q(p) \right| \tag{24}$$

$$q(p) = ln \, ln \, \left(\frac{r_{21}^p - s}{r_{32}^p - s} \right) \tag{25}$$

$$s = 1 * sgn \left(\frac{\varepsilon_{32}}{\varepsilon_{21}} \right) \tag{26}$$

$$\varepsilon_{32} = \phi_3 - \phi_2 \; ; \; \varepsilon_{21} = \phi_2 - \phi_1 \tag{27}$$

ϕ_k is the solution of k th grid. That can be selected as a scalar value from a solution such as a sway force. ε_{21} and ε_{32} have been calculated with the help of the Equation (27) and these parameters used to calculation of s in Equation (26). The negative value of s means oscillatory convergence. The apparent order, p, has been calculated with the help of Equation (24) and (25). As can be seen in equation (24) there is a function related to p, which is $q(p)$, in equation p. For this reason, an initial estimate was made while calculating p, and p was found iteratively.

$$R = \frac{\varepsilon_{21}}{\varepsilon_{32}} \tag{28}$$

The convergence factor R can be obtained with the help of Equation (28).

$$\phi_{ext}^{21} = \frac{\left(r_{21}^p \phi_1 - \phi_2\right)}{r_{21}^p - 1} \tag{29}$$

ϕ_{ext}^{21} in Equation (29) is extrapolated scalar value of selected ϕ.

$$e_a^{21} = \left|\frac{\phi_1 - \phi_2}{\phi_1}\right| \tag{30}$$

$$e_{ext}^{21} = \left|\frac{\phi_{ext}^{21} - \phi_1}{\phi_{ext}^{21}}\right| \tag{31}$$

e_a^{21} is the approximate error while e_{ext}^{21} is extrapolated error.

$$GCI_{fine}^{21} = \frac{1.25 * e_a^{21}}{r_{21}^p - 1} \tag{32}$$

The Grid Convergence Index (GCI) can be found with Equation (32).

Uncertainty analysis results are given in Table 3. When the data in Table 2 and Figures 7 and 8 are examined, it is seen that the error rate stabilized after Mesh 4. The number of cells, which directly affects the computational cost, increases approximately 1.9 times between Mesh 4 and Mesh 5. The solution time is significant in terms of computational cost, since the selected mesh will be used in the analyses which will be done in the next part of the study. Considering the capacity of the computer used, the change in the error rate was ignored and Mesh 4 was chosen.

5. RESISTANCE ANALYSES

The full-scale geometry of the 7m length submarine is used in the resistance analyses. The mesh sizes used in the resistance analyses are the same as those obtained from the Mesh 4 mesh structure in the mesh independence study conducted for static drift analyses. The flow volume is recreated to be proportional to the full-scale size. As a result, there is an increase in the number of meshes. Four different analyses are conducted at speeds of 0.5, 1.0, 1.5, and 2.0 m/s. The results of these analyses can be seen in the Table 4 and Figure 9. The velocity distribution around the Autosub geometry can be seen in Figure 10.

As can be seen in Table 4, the empirical results presented by Phillips et al. (2007) do not match with the test results performed by Fallows (2004). In the experiment conducted by Fallows (2004), the 2.5 m. length model was drawn from the water surface at a depth of 2.6 diameter. This means that the submarine is close to the water surface and produces waves (Phillips et al., 2009). In addition, a model

Table 3. Spatial Uncertainty

	Sway Force (Y) [N]	Yaw Moment (N) [N-m]
N_1	5639856	
N_2	2952064	
N_3	1841095	
N_4	117085	
N_5	794489	
r_{21}	1,2433	
r_{32}	1,1605	
ϕ_1	300,4577	300,3557
ϕ_2	301,7904	302,1399
ϕ_3	305,4607	303,9573
p	5,5636	1,7453
R	0,3631	0,9817
ϕ_{ext}^{21}	299,8925	296,4963
e_a^{21}	0,44%	0,59%
e_{ext}^{21}	0,19%	1,3%
GCI_{mesh5}^{21}	0,24%	1,6%

Table 4. Resistance Results

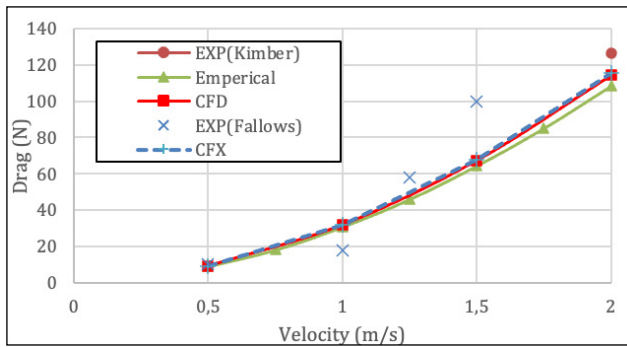| Velocity (m/s)	EXP (Fallows)	EXP (Kimber)	Empirical (Phillips et al.)	CFX (Phillips et al.)	CFD	Error % Empirical	Error % CFX
0,5	10,337	-	9,003	8,943	9,175	1,912	2,589
0,75	-	-	18,061		-		
1	18,023	-	30,663	31,959	31,873	3,941	-0,270
1,25	58,064	-	45,886		-		
1,5	100,017	-	64,242	67,926	67,328	4,801	-0,881
1,75	-	-	84,898		-		
2	-	126,6494	108,228	115,531	114,376	5,683	-1,001

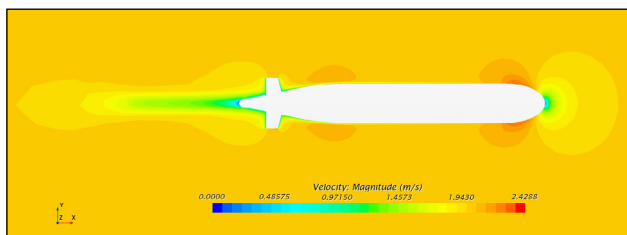**Figure 9.** Comparisons of resistance predictions for Autosub (Phillips et al., 2007).

Figure 10. Velocity Magnitude for Resistance.

Figure 11. Variation of Sway Force (Y') with Sway Velocity (v').
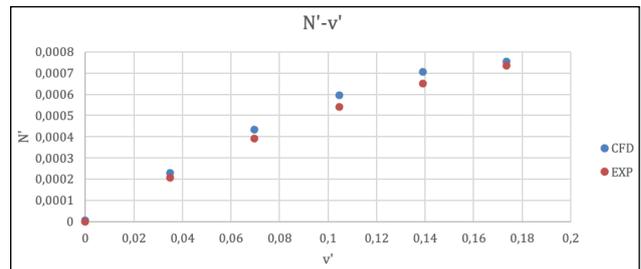
Figure 12. Variation of Yaw Moment (N') with Sway Velocity (v').

with a length of 2.5 meters was used in the experiment. As the speed increases, the increase in the margin of error supports that the factor causing this difference is the wave resistance. In the thesis published by Fallows, these problems related to the test setup were mentioned. Another cause of error is the presence of a large mounting post on the test setup. The forces caused by this structure affected the test results. These reasons are the causes for the difference between experimental results (Fallows, 2004), CFD results and empirical results. On the other hand, the CFD result for 2m/s agrees with the experimental results from Kimber&Marshfield (1993) with an error rate of %10. Also, the CFD results have error rates less than %6 with the empirical results (Phillips et al., 2007). In addition to these the results match with the CFX solution made by Phillips et al. (2007) with an error rate of less than %2,6.
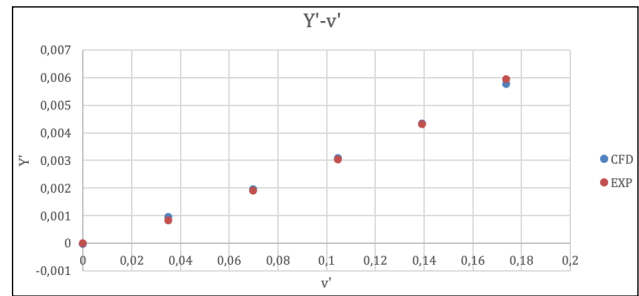
6. STATIC DRIFT ANALYSES

Six further analyses are performed for the static drift condition at angles of 0, 2, 4, 6, 8, and 10 degrees, with a velocity of 2.69 m/s. The obtained results are compared with the experimental data from Kimber&Marshfield (1993). Static drift results are presented in Table 5. The hydrodynamic sway force Y' and yaw moment N' are presented in Figure 11 and 12.

Figures 13, 14, 15, and 16 show the results obtained from the CFD analysis. The highest and lowest values in the obtained results differ by changing the static drift angle. However, to provide a comparative result, the velocity and pressure range are limited to a single value for each figure.

Figure 13 shows the flow field around the submarine. It is seen that the characteristic of the flow around the submarine changes as the static drift angle increases.

Table 5. Static Drift Results

| AoA	v' (Sway Velocity)	Y'	N'	Y'(EXP)	N'(EXP)	Error (%) Y'	Error (%) N'
0	0	-1,2E-05	5,85E-06	0	0	-	-
2	0,0348995	0,00095	0,000231	0,000836	0,000206	13,65061	12,14809
4	0,0697565	0,001969	0,000433	0,001913	0,000391	2,928268	10,677273
6	0,1045285	0,00309	0,000595	0,003032	0,00054	1,910778	10,268147
8	0,1391731	0,004343	0,000707	0,004305	0,000652	0,877556	8,4381988
10	0,1736482	0,005769	0,000756	0,005931	0,000734	-2,73295	2,8820465
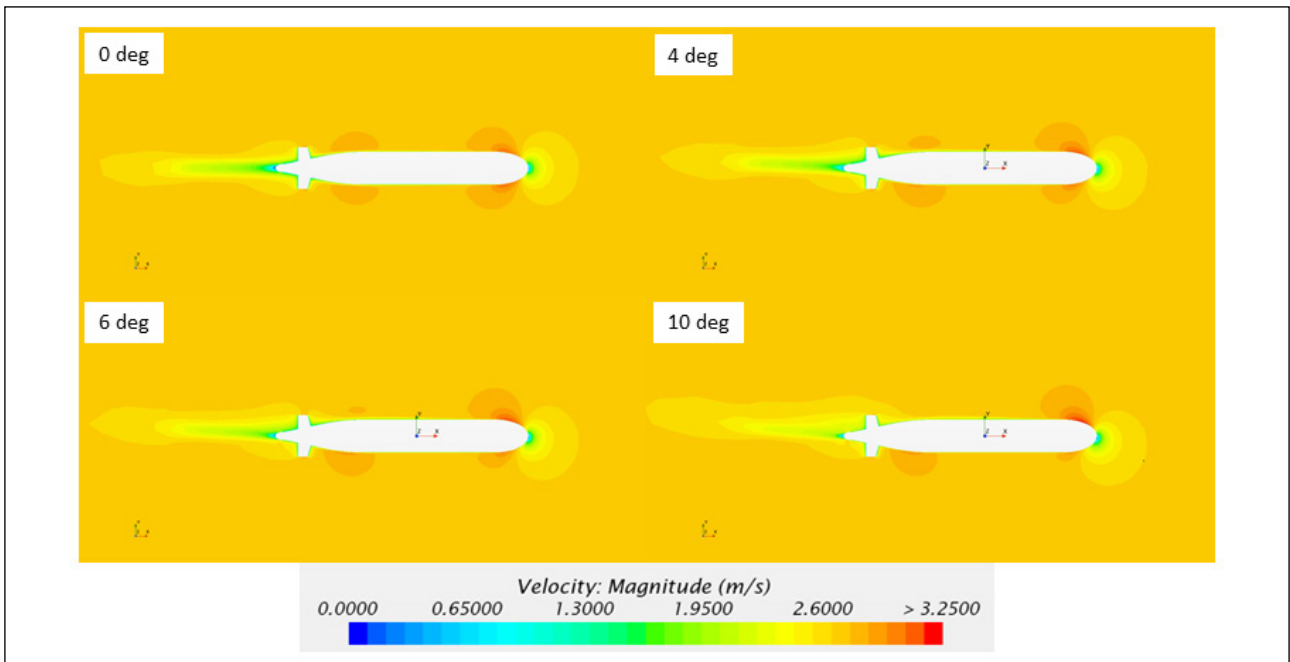
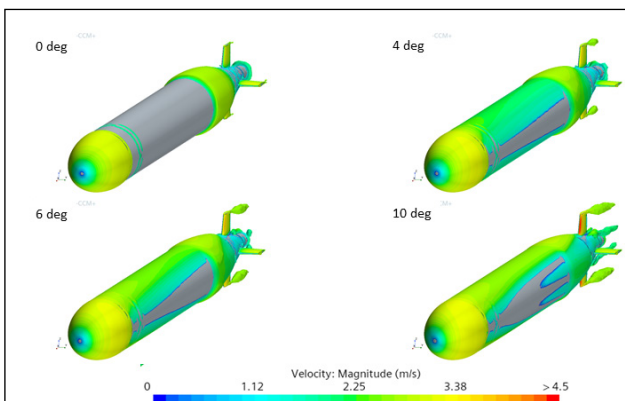**Figure 13.** Velocity Distribution Around the Submarine.

Figure 14. Q Criteria = 5 Surfaces Around the Submarine.

Surfaces with a Q-Criteria value equal to 5 were obtained. The velocity distribution on these surfaces is shown in Figure 14. The Q-Criteria value allows us to examine the wake behind the submarine. As can be seen, as the angle increases, the maximum velocity obtained increase, and the angle of the wake and length of the wake also increases.

Figure 15 shows the streamline drawn from the submarine surfaces. When the submarine is subjected to a static drift angle, a rotational flow is observed around it. As this angle increases, it is seen in the figures that the streamlines in the rear part of the submarine are more complex and have higher velocity.
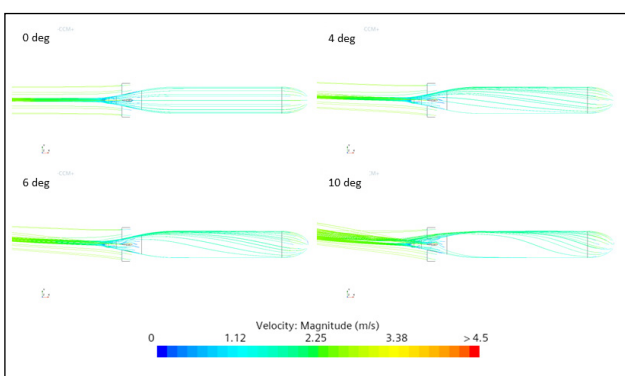
Figure 16 shows the fins in the aft body of the submarine. The pressure distribution over these fins changes as the angle changes. As the angle increases, the region of
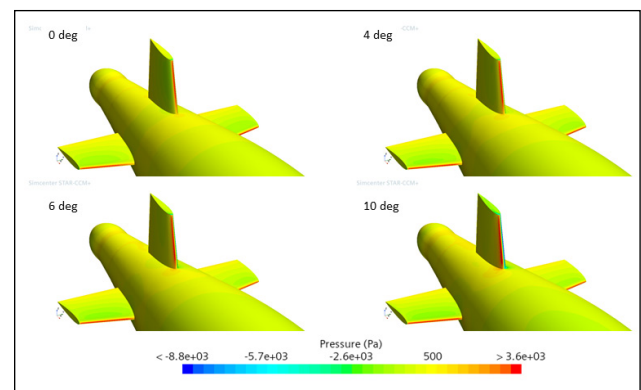

Figure 15. Streamlines Around the Submarine.

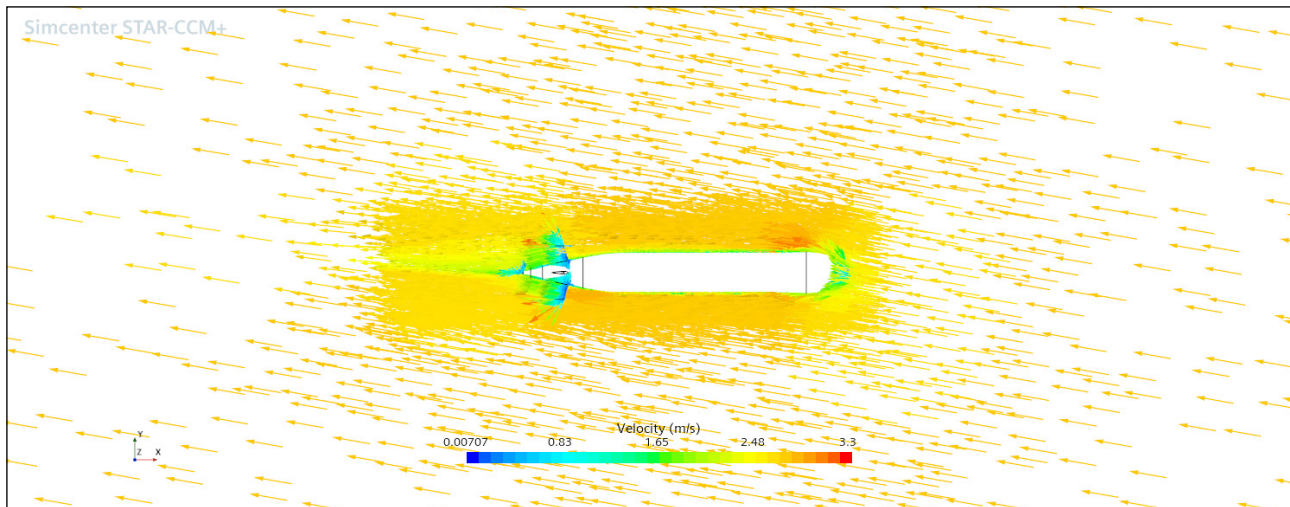**Figure 16.** Pressure Distribution on Aft Body of Submarine.

Figure 17. Vector Field Around the Submarine.

maximum pressure on the fin is displaced. This causes an increase in the force created by the fins as the angle increases. This effect is one of the reasons why the yaw moment increases as the angle increases.

The vector field around the submarine is shown in Figure 17. In this image given for the 10-degree static drift condition, the angle of the flow acting on the submarine is clearly seen. The resulting sway force and yaw moment are caused by the flow of the body acting at a certain angle. It is seen that it reaches 3.3 m/s in the cross section of this image performed at a speed of 2.69 m/s. These velocity zones affect the pressure zones around the submarine, causing sway force and yaw moment to occur.

When comparing the force and moment values obtained through CFD with experimental results, it is observed that the error rates vary between -5% and 10% (Table 5). The results (Figure 11 and Figure 12) presented show that the sway forces and yaw moments obtained from the analyze give independent results from the mesh structure and are in consistency with the experimental results presented in the literature. As a result, an analysis method that can be used in future studies has been presented.

7. CONCLUSIONS

This study involves the force and moment calculations of the Autosub submarine using model and full-scale geometries. The RANS equations and two-equation turbulence models are employed in the calculations. Static drift analyses are conducted for angles of 0, 2, 4, 6, 8, and 10 degrees. The calculations are performed at a cruising speed of 2.69 m/s using a scale factor of 1.346. To determine the optimum mesh structure, a mesh independence study is carried out at 6 degrees static drift angle. The error rates of the experimental results and the calculated values in the analysis are used in the mesh independence study. After determining the optimum mesh structure with the help of the

uncertainty analyses and the mesh independence study, the analyses are completed for other angles and compared with the experimental results.

Full-scale resistance analyses are conducted using the same mesh sizes. Resistance analyses are performed for the 7m full-scale geometry at velocities of 0.5, 1.0, 1.5, and 2.0 m/s. The calculated resistance forces are compared with the experimental results. There are two experimental results for resistance presented in the open literature. In the first presented by Kimber&Marshall (1993) a resistance value for 2 m/s is available, while Fallows (2004) presented the resistance values for a larger range. The experimental results of Fallows cover speeds ranging from 0 to 5 m/s for different model depths so that the wave resistance is also included in the values. So, there is a deviation from the experimental results comparing to CFD, empirical and also experimental result obtained before by Kimber&Marshall (1993). The cause of this deviation is also discussed by Phillips et al. (2007). The CFD results of the present study appear to be in good agreement with the CFD results presented by Phillips et al. (2007), as well as the experimental results by Kimber & Marshall (1993), with an error rate of 2.6% and 10%, respectively.

The static drift analyses are conducted for different drift angles and a good agreement is seen with the experimental results conducted by Kimber&Marshall (1993). While the deviation from the experimental results is lesser in the sway forces more deviation is seen for the yaw moment. However, the deviation is in an acceptable level since 10 % of deviation is seen.

The force and moment values obtained from the static drift and resistance analyses are found to be consistent with the experimental and empirical results available in the literature with an error ratio of %0.8-%13.5 and %1.9-%5.6, respectively.

It is seen that the pure sway forces and pure yaw moments can be obtained with high accuracy with CFD methods. The mesh independence study and the validation study show that the numerical results are consistent with the experimental results. This shows that the method used in this study can be used for the predictions of hydrodynamic coefficients for static drift condition. In future studies the method will be used for derived geometries of the Autosub submarine for different L/B ratios.

DATA AVAILABILITY STATEMENT

The published publication includes all graphics and data collected or developed during the study.

CONFLICT OF INTEREST

The author declared no potential conflicts of interest with respect to the research, authorship, and/or publication of this article.

ETHICS

There are no ethical issues with the publication of this manuscript.

FINANCIAL DISCLOSURE

The authors declared that this study has received no financial support.

REFERENCES

Abkowitz, M. A. (1964). *Lectures on Ship Hydrodynamics Steering and Maneuverability Technical Report. Hydro and Aerodynamic Laboratory, Lyngby, Denmark.* Technical Report Hy-5.

Ackermann, S. (2008). *Prediction of Suboff Hydrodynamics using ANSYS CFX Software. Launceston.* National Centre of Maritime Engineering and Hydrodynamics.

Alin, N., Bensow, R., Fureby, C., & Huuva, T. (2010). Current Capabilities of DES and LES for Submarines at Straight Course. *Journal of Ship Research, 54*, 184–196.

Arslan, S. (2013). Su altı araçları için yeni geliştirilen hidrodinamik modelleme yöntemleri kullanılarak otonom bir su altı aracının hidrodinamik karakteristiğinin incelenmesi. [Master Thesis]. Istanbul Technical University.

Atik, H. (2021). Türbülans modellerinin DARPA SUBOFF statik sürükleme testi üzerinden incelenmesi. *Gazi Üniversitesi Mühendislik-Mimarlık Fakültesi Dergisi, 3,* 1509–1522. [CrossRef]

Bull, P. (1996). *The validation of CFD predictions of nominal wake for the SUBOFF fully appended geometry.* 21st Symposium on Naval Hydrodynamics, Trondheim, Norway, 1061–1076.

Can, M. (2014). *Numerical simulation of hydrodynamic planar motion mechanism test for underwater vehicles* [Master Thesis]. The Graduate School of Natural and Applied Sciences of Middle East Technical University.

Cardenas, P., & de Barros, E. A. (2019). Estimation of AUV Hydrodynamic Coefficients Using Analytical and System Identification Approaches. *IEEE Journal of Oceanic Engineering, 1–20.*

Carrica, P. M., Kerkvliet, M., Quadvlieg, F., & Martin, J. E. (2016). *CFD Simulations and Experiments of a Maneuvering Generic Submarine and Prognosis for Simulation of Near Surface Operation.* 31st Symp. Nav. Hydrodyn. (ONR), Monterey, CA, 11–16.

Carrica, P. M., Kim, Y., & Martin, J. E. (2019). Near-surface self propulsion of a generic submarine in calm water and waves. *Ocean Engineering, 183,* 87–105. [CrossRef]

Celik, I., Ghina, U., Roache, P., Fretias, C.J., & Raad, H.C.P.E. (2008). Procedure for estimation and reporting of uncertainty due to discretization in CFD applications. *Journal of Fluids Engineering, 130*(7), Article 078001. [CrossRef]

Chase, N., & Carrica, P. M. (2013). Submarine propeller computations and application to self-Propulsion of DARPA suboff, *Ocean Engineering, 60,* 68–80. [CrossRef]

Crook, L.B. (1990). *Resistance for DARPA SUBOFF as Represented by Model 5470.* DTRC/SHD-1298-07.

Davidson, K. S. M., & Schiff, L. I. (1946). Turning and course keeping qualities. *Trans Soc Nav Archit Mar Eng*, 54.

Duman, S., Sezen, S., & Bal, S. (2018). *Propeller Effects on Maneuvering of a Submerged Body. A. Yücel Odabaşı Colloquium Series 3 rd International Meeting - Progress in Propeller Cavitation and its Consequences: Experimental and Computational Methods for Predictions.* 15th – 16th November, Istanbul, Turkey.

Efremov, D. V., & Milanov, E. M. (2019). Hydrodynamics of DARPA SUBOFF submarine at shallowly immersion conditions. In: TransNav: *International Journal on Marine Navigation and Safety of Sea Transportation, 13*, 2. [CrossRef]

Fallows, C. D. (2004). Characterization of the propulsion system of autonomous underwater vehicles. [Doctorial dissertation]. University of Southampton.

Fell, B. J. (2009). *Structured Mesh Optimization and CFD Simulation of the Fully Appended DARPA Suboff Model* [Master Thesis]. University of Tasmania, National Centre for Maritime Engineering and Hydrodynamics.

Gertler, M., Hagen, G. (1967). *Standard equations of motion for submarine simulation.* Technical Report AD653861, [CrossRef]

Groves, N.C., Huang, T.T., & Chang, M.S. (1989). *Geometric Characteristics of Darpa Suboff Models, David Taylor Research Center, Ship Hydromechanics* Department, Report Number DTRC/SHD-1298-01.

ITTC Resistance Committee. (2017). *Uncertainty analysis in CFD Verification and validation methodology and procedures.* ITTC - Recomm. Proced. Guidel., p. 1–13.

Joung TH., Sammut, K., He, F., & Lee, SK. (2012). Shape optimization of an autonomous underwater vehicle with a ducted propeller using computational fluid dynamics analysis. *International Journal of Naval Architecture and Ocean Engineering, 4,* 44–56. [CrossRef]

Kahramanoglu, E. (2023). Numerical investigation of the scale effect on the horizontal maneuvering derivatives of an underwater vehicle. *Ocean Enginering, 272,* Article 113883. [CrossRef]

Kırıkbaş, O, Kınacı, Ö. K., & Bal, Ş. (2021a). Sualtı araçlarının manevra karakteristiklerinin değerlendirilmesi-i: manevra analizlerinde kullanılan yaklaşımlar. *GMO Journal of Ship and Marine Technology, 219,* 6–58.

Kırıkbaş, O, Kınacı, Ö. K., & Bal, Ş. (2021b). Su altı araçlarının manevra karakteristiklerinin değerlendirilmesi-ii: akışkan sınırlarının etkileri. *GMO Journal of Ship and Marine Technology, 220,* 135–174. [CrossRef]

Kimber, N., & Marshfield, W. (1993). *Design and testing of control surfaces for the autosub demonstrator test vehicle.* Technical report, DRA Haslar.

Liu, H., & Huang, T. (1998). *Summary of DARPA SUBOFF experimental program data.* Report No. CRDKNSWC/HD-1298-11. [CrossRef]

Mackay, M. (1988). *Flow Visualization Experiments with Submarine Models in a Wind Tunnel, Defence Research Establishment Atlantic.* Technical Memorandum 88/204.

McDonald, H., Whitfield, D. (1996). *Self-propelled maneuvering underwater vehicles.* 21st Symposium on Naval Hydrodynamics, Trondheim.

Phillips, A., Furlong, M., &Turnock, S.R. (2007). *The use of Computational Fluid Dynamics to Determine the Dynamic Stability of an Autonomous Underwater Vehicle.* file:///Users/kareyayincilik11/Downloads/The_use_of_Computational_Fluid_Dynamics_to_Determi%20(1).pdf. Accessed on Dec 17, 2023. [CrossRef]

Phillips, A., Furlong, M., & Turnock, S.R. (2010). *Virtual planar motion mechanism tests of the autonomous underwater vehicle autosub.* STG-Conference /

Lectureday "CFD in Ship Design", 2007.

Phillips, A., Furlong, M., & Turnock, S. R. (2011). The use of computational fluid dynamics to aid cost-effective hydrodynamic design of autonomous underwater vehicles. *Sage Journals, 224*(4), 239–254. [CrossRef]

Roache, P. J. (1998). Verification of codes and calculations. *AIAA Journal, 36(5),* 696–702. [CrossRef]

Roddy, R.F. (1990). *Investigation of the Stability and Control Characteristics of Several Configurations of the DARPA SUBOFF Model (DTRC 5470) from Captive-Model Experiments.* DTRC/SHD-1298-08.

Saeidinezhad, A., Dehghan, A. A., & Manshadi, M. D. (2015). Experimental investigation of hydrodynamic characteristics of a submersible vehicle model with a non-axisymmetric nose in pitch maneuver. *Ocean Engineering, 100,* 26–34. [CrossRef]

SNAME. (1950). *Nomenclature for treating the motion of a submerged body through a fluid* (Technical and Research Bulletin No. 1–5). SNAME.

Thomas, R. (2003). *Performance evaluation of the propulsion system for the autonomous underwater vehicle C-scout* [Unpublished Master Thesis]. Faculty of Engineering and Applied Science Memorial University of Newfoundland.

Thomas, R., Bose, N., & Williams, D. (2003). Propulsive Performance of the Autonomous Underwater Vehicle C-Scout. OCEANS 2003, San Diego, ABD.

Toxopeus, S., & Vaz, G. (2009). *Calculation of Current or Maneuvering Forces using a Viscous-Flow Solver. In Proceedings of OMAE2009*, Honolulu, Hawaii, USA. [CrossRef]

Vaz, G., Toxopeus, S., & Holmes, S. (2010). *Calculation of Maneuvering Forces on Submarines Using Two Viscous-Flow Solvers'*, OMAE 2010, Shanghai, China. [CrossRef]

Zhao, B., Yun, Y., Hu, F., Sun, J., Wu, D., & Huang, B. (2022). Hydrodynamic coefficients of the DARPA SUBOFF AFF-8 in rotating arm maneuver: Part I: Test technology and validation. *Ocean Engineering, 266,* Article 113148. [CrossRef]

Wu, C. S., He, S. I., Zhu, D. X., & Min, G. (2006). Numerical simulation of microbubble flow around an axisymmetric body. *Journal of Hydrodynamics, 18*(3), 217–222. [CrossRef]